



This is a repository copy of *Formation of Jupiter-mass binary objects through photoerosion of fragmenting cores.*

White Rose Research Online URL for this paper:

<https://eprints.whiterose.ac.uk/219466/>

Version: Published Version

Article:

Diamond, J.L. and Parker, R.J. orcid.org/0000-0002-1474-7848 (2024) Formation of Jupiter-mass binary objects through photoerosion of fragmenting cores. *The Astrophysical Journal*, 975 (2). 204. ISSN 0004-637X

<https://doi.org/10.3847/1538-4357/ad8644>

Reuse

This article is distributed under the terms of the Creative Commons Attribution (CC BY) licence. This licence allows you to distribute, remix, tweak, and build upon the work, even commercially, as long as you credit the authors for the original work. More information and the full terms of the licence here:

<https://creativecommons.org/licenses/>

Takedown

If you consider content in White Rose Research Online to be in breach of UK law, please notify us by emailing eprints@whiterose.ac.uk including the URL of the record and the reason for the withdrawal request.



eprints@whiterose.ac.uk
<https://eprints.whiterose.ac.uk/>



Formation of Jupiter-mass Binary Objects through Photoerosion of Fragmenting Cores

Jessica L. Diamond and Richard J. Parker¹ Astrophysics Research Cluster, School of Mathematical and Physical Sciences, The University of Sheffield, Hicks Building, Hounsfield Road, Sheffield, S3 7RH, UK; R.Parker@sheffield.ac.uk*Received 2024 June 20; revised 2024 October 10; accepted 2024 October 10; published 2024 November 5*

Abstract

The recent discovery of tens of Jupiter-mass binary objects (JuMBOs) in the Orion Nebula Cluster (ONC) with the James Webb Space Telescope has intensified the debate on the origin of free-floating planetary mass objects within star-forming regions. The JuMBOs have masses below the opacity limit for fragmentation but have very wide separations (from tens to hundreds of astronomical units), suggesting that they did not form in a similar manner to other substellar mass binaries. Here, we propose that the theory of photoerosion of prestellar cores by Lyman continuum radiation from massive stars could explain the JuMBOs in the ONC. We find that for a range of gas densities the final substellar mass is comfortably within the JuMBO mass range, and the separations of the JuMBOs are consistent with those of more massive (G- and A-type) binaries, which would have formed from the fragmentation of the cores had they not been photoeroded. The photoerosion mechanism is most effective within the H II region(s) driven by the massive star(s). The majority of the observed JuMBOs lie outside of these regions in the ONC, but they may have formed within them and then subsequently migrated due to dynamical evolution.

Unified Astronomy Thesaurus concepts: [Star forming regions \(1565\)](#); [Massive stars \(732\)](#); [Star formation \(1569\)](#); [Brown dwarfs \(185\)](#); [Free floating planets \(549\)](#); [H II regions \(694\)](#)

1. Introduction

Understanding the formation mechanism(s) of brown dwarfs and planetary-mass objects is one of the current outstanding problems in astrophysics. It is difficult to explain the formation of planets more than several Jupiter masses (M_{Jup}) via the core-accretion theory of planet formation (J. B. Pollack et al. 1996; G. Chabrier et al. 2014), and it is also difficult to explain the formation of significant numbers of free-floating planetary-mass objects via collapse and fragmentation, as the opacity limit for fragmentation reaches a minimum at around $10 M_{\text{Jup}}$ (M. J. Rees 1976; P. Padoan & A. Nordlund 2004; M. R. Bate 2012; P. Hennebelle & G. Chabrier 2013; P. C. Clark & A. P. Whitworth 2021).

The discovery of 540 free-floating Jupiter-mass objects in the Orion Nebula Cluster (ONC) with the James Webb Space Telescope (JWST; S. G. Pearson & M. J. McCaughrean 2023) was therefore unexpected, especially given so many of these objects (42) are apparently in binary systems with both components of the binary in the mass range $0.7\text{--}13 M_{\text{Jup}}$ (hence the moniker “Jupiter-mass binary object”—or “JuMBO” for short).

Furthermore, the fraction of these systems in binaries is much higher (at around 9%; S. G. Pearson & M. J. McCaughrean 2023) than for other, slightly more massive substellar objects over a similar separation range (10s–100s au), which appears to be inconsistent with the previously observed trend of decreasing multiplicity fraction with decreasing primary mass (G. Duchêne & A. Kraus 2013).

While there are many different formation theories for brown dwarfs (e.g., B. Reipurth & C. Clarke 2001; A. P. Whitworth & H. Zinnecker 2004; G. F. Gahm et al. 2007; S. P. Goodwin &

A. P. Whitworth 2007; M. R. Bate 2009; T. J. Haworth et al. 2015; S. S. Mathew & C. Federrath 2021), most do not predict that the brown dwarfs would form in a binary system, and the fraction of planetary-mass objects in binaries in the S. G. Pearson & M. J. McCaughrean (2023) sample exceeds the binary fraction for more massive brown dwarf–brown dwarf (BD–BD) binaries in the Galactic field (G. Basri & A. Reiners 2006; A. J. Burgasser et al. 2007; I. Thies & P. Kroupa 2007). Furthermore, the separation distribution on the JuMBOs is skewed toward significantly higher values (28–384 au) than the BD–BD binaries in the field (~ 4 au; A. J. Burgasser et al. 2007) and in fact is more similar to the peak separations of higher-mass binary systems (e.g., K, F, and G type, i.e., $0.5\text{--}1.5 M_{\odot}$, or A type, i.e., $1.5\text{--}3.0 M_{\odot}$, which peak at ~ 50 and ~ 300 au, respectively; D. Raghavan et al. 2010; R. J. De Rosa et al. 2014).

While S. G. Pearson & M. J. McCaughrean (2023) note the apparent difficulty in explaining the formation of such low-mass binary objects (though several authors have proposed various dynamical mechanisms for their formation; e.g., C. Lazzoni et al. 2024; S. Portegies Zwart & E. Hochart 2024; Y. Wang et al. 2024), the environment of the ONC—with its massive stars driving H II regions (C. R. O’Dell et al. 2017; S.-J. Kang et al. 2017; C. R. O’Dell et al. 2020; E. Habart et al. 2024)—is conducive to forming low-mass objects via the photoerosion of prestellar cores (A. P. Whitworth & H. Zinnecker 2004).

In the A. P. Whitworth & H. Zinnecker (2004) theory (see also J. E. Dyson 1968; F. D. Kahn 1969; J. J. Hester et al. 1996; G. F. Gahm et al. 2007), Lyman continuum radiation from massive stars drives an ionization shock front into the prestellar core, compressing the inner layers while simultaneously evaporating the outer layers. The net effect is a very efficient formation of a substellar-mass object. While A. P. Whitworth & H. Zinnecker (2004) describe the formation of a single object, the multiplicity of protostars is high (e.g., X. Chen et al. 2013), and so the formation of a substellar

¹ Royal Society Dorothy Hodgkin Fellow.

system via photoerosion might act on a primordial binary system.

In this paper, we use the theory in A. P. Whitworth & H. Zinnecker (2004) to calculate the mass of a substellar object formed via photoerosion of a prestellar core by radiation from massive stars. For each core that could form one or more substellar objects, we then calculate the likely primary mass of the binary system that would have formed had the core not been photoeroded.

The paper is organized as follows. In Section 2, we outline the theory and describe the properties of the various types of binary systems we will compare our results to. We present our results in Section 3, and we discuss them in Section 4. We conclude in Section 5.

2. Method

Our starting assumption is that the photoerosion mechanism described in A. P. Whitworth & H. Zinnecker (2004) would act on a core that was already starting to fragment to form a binary or multiple system. We assume that the same amount of mass would be lost from the core during photoerosion but that the final system would be a binary object, rather than a single object.

Stellar binaries are thought to predominantly form either through the turbulent fragmentation of a prestellar core (e.g., E. J. Delgado-Donate et al. 2004; S. P. Goodwin et al. 2007; M. R. Bate 2009; S. S. R. Offner et al. 2010; M. R. Bate 2012), or (less often) the fragmentation of a circumstellar disk (e.g., W. K. M. Rice et al. 2005; D. Stamatellos & A. P. Whitworth 2009). The timescales for the initial fragmentation are short (high multiplicity fractions are found in young (≤ 0.1 Myr) protostellar cores; e.g., X. Chen et al. 2013; Q.-y. Luo et al. 2022), and we can compare this to the timescales for the core photoerosion model in A. P. Whitworth & H. Zinnecker (2004).

A. P. Whitworth & H. Zinnecker (2004) determine that the timescale for the first stage of the erosion (t_1 , the time taken for the inward propagation wave to erode the outer core and compress the center) is given by

$$t_1 = \frac{1}{(2\pi G n_0 m)^{1/2}}, \quad (1)$$

where $m = m_p/X$, the mass associated with one hydrogen nucleus (m_p is the proton mass and X the mass fraction of hydrogen), and n_0 is the density of hydrogen nuclei in the H II region surrounding the core. We adopt two different hydrogen nucleus densities, $n_0 = 10^3$ and $n_0 = 10^4 \text{ cm}^{-3}$, which give either $t_1 \sim 1$ or $t_1 \sim 0.3$ Myr, respectively. Both of these timescales are higher than the timescale for initial fragmentation (~ 0.1 Myr), suggesting that the process of forming the would-be stellar binary has already been set in motion before the photoerosion takes hold.

However, we contend that photoerosion could still influence the final mass of the binary system. The initial fragmentation of the core into a binary system occurs after ~ 0.1 Myr, but in simulations, S. P. Goodwin et al. (2004) and M. R. Bate (2009) show that a significant proportion of the binary component masses (up to several M_\odot) is accreted in the subsequent ~ 0.1 – 0.3 Myr. Therefore, the core can fragment into a (low-mass) protobinary system, but photoerosion will act to remove the material that would otherwise be accreted onto the binary system on a timescale that is similar to, or faster than, the

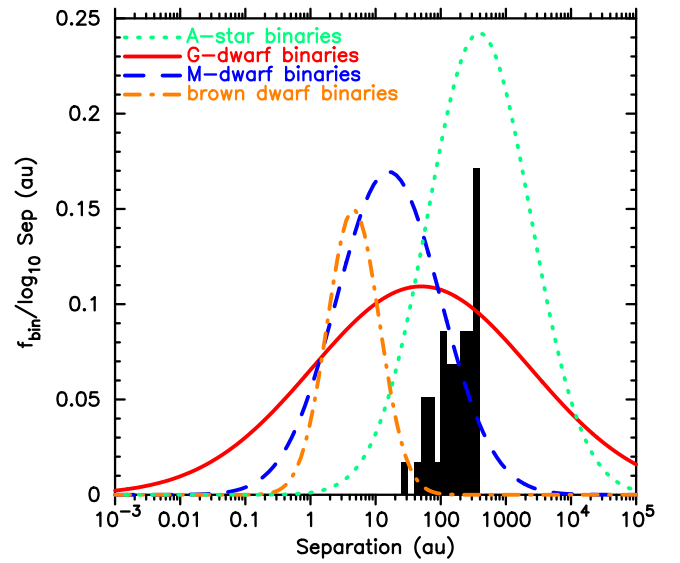


Figure 1. Separation distribution of the JuMBOs (the black histogram). For comparison, we show the Gaussian fits to the separation distributions of various stellar and substellar binary populations. The fit to the brown dwarf–brown dwarf binaries (A. J. Burgasser et al. 2007; I. Thies & P. Kroupa 2007) is shown by the dotted–dashed orange line, the fit to the M-dwarf binaries (C. Bergfors et al. 2010; M. Janson et al. 2012) is shown by the dashed blue line, the fit to the G-dwarf (solar-type) binaries (D. Raghavan et al. 2010) is shown by the solid red line, and the fit to the A-type binaries (R. J. De Rosa et al. 2014) is shown by the dotted green line.

accretion timescale. The net effect of this process is to reduce the final mass of the components of the binary.

In Figure 1, we show the separation distribution of the JuMBOs from S. G. Pearson & M. J. McCaughrean (2023) via the black histogram. For comparison, we show Gaussian fits to the separation distributions of stellar-mass binaries observed in the Galactic field (the dashed blue (M-type), solid red (G-type), and dotted green (A-type) lines), as well as the Gaussian fit to the BD–BD binary separation distribution (the dotted–dashed orange line). The latter is mainly for systems in the Galactic field, although it does include several examples from nearby star-forming regions (R. J. Parker & S. P. Goodwin 2011). A summary of these distributions (i.e., the mean separation, and the variance of the Gaussian fit, and the primary mass range the fits are valid for) is given in Table 1.

We also assume the core mass function is the precursor to the stellar initial mass function (IMF; J. Alves et al. 2007) but shifted to higher masses by a factor equal to the inverse of the star formation efficiency, ϵ . We set $\epsilon = 0.333$ and draw $N_{\text{core}} = 1000$ masses from a core mass function that has the same shape as the T. Maschberger (2013) stellar IMF,

$$p(m) \propto \left(\frac{m}{\mu}\right)^{-\alpha} \left(1 + \left(\frac{m}{\mu}\right)^{1-\alpha}\right)^{-\beta}. \quad (2)$$

In Equation (2), $\alpha = 2.3$ is the E. E. Salpeter (1955) power-law exponent for higher-mass cores, and $\beta = 1.4$ describes the turnover at lower masses. As the core mass function is shifted to higher masses (by a factor of $1/\epsilon$) compared to the stellar IMF, we adopt $\mu = 0.6 M_\odot$ and sample masses in the range $M_{\text{core}} = 0.3$ – $300 M_\odot$.

For each core mass, M_{core} , we use the analytical formulae from A. P. Whitworth & H. Zinnecker (2004) to estimate the

Table 1
Stellar and Substellar Binary Properties Compared with the Properties of the JuMBOs

Type	Primary Mass	f_{bin}	\bar{a} (au)	$\log \bar{a}$	$\sigma_{\log \bar{a}}$	References	Color
BD	$0.02 < m_p / M_{\odot} \leq 0.08$	0.15	4.6	0.66	0.4	A. J. Burgasser et al. (2007) and I. Thies & P. Kroupa (2007)	Orange
M	$0.08 < m_p / M_{\odot} \leq 0.45$	0.34	16	1.20	0.80	C. Bergfors et al. (2010) and M. Janson et al. (2012)	Blue
G	$0.8 < m_p / M_{\odot} \leq 1.2$	0.46	50	1.70	1.68	D. Raghavan et al. (2010)	Red
A	$1.5 < m_p / M_{\odot} \leq 3.0$	0.48	389	2.59	0.79	R. J. De Rosa et al. (2014)	Green

Note. We show the type of the primary mass m_p , the main-sequence mass range this corresponds to, the binary fraction f_{bin} , the mean separation \bar{a} , and the mean ($\log \bar{a}$) and variance ($\sigma_{\log \bar{a}}$) of the log-normal fits to these distributions. The final column indicates the color of each corresponding line in Figure 1.

final mass of the photoeroded core, M_3 ,

$$M_3 \simeq \frac{2f\alpha_*GM_{\text{core}}^2}{3\alpha_1a_{\text{II}}^2R_{\text{HII}}}, \quad (3)$$

where $f=1.7$ is a factor that takes into account accretion from the remaining envelope of the core onto the low-mass object, and G is the gravitational constant. $\alpha_* = 2 \times 10^{-13} \text{ cm}^3 \text{ s}^{-1}$ is the recombination coefficient into excited states, and $\alpha_1 = 10^{-13} \text{ cm}^3 \text{ s}^{-1}$ is the recombination coefficient into the ground state only. $a_{\text{II}} = 10^6 \text{ cm s}^{-1}$ is the isothermal speed of sound in an ionized gas, and R_{HII} is the radius of the H II region within which the core is being photoeroded.

The size of the H II region, R_{HII} , is given by

$$R_{\text{HII}} = \left(\frac{3\dot{N}_{\text{Lyc}}}{4\pi\alpha_*n_0^2} \right)^{1/3}, \quad (4)$$

where \dot{N}_{Lyc} is the Lyman continuum photon rate from the massive star(s) and n_0 is the number density of hydrogen nuclei. While A. P. Whitworth & H. Zinnecker (2004) present results for a wide range of the parameter space, we fix a_{II} but adopt two values for the density of hydrogen nuclei, $n_0 = 10^3$ and $n_0 = 10^4 \text{ cm}^{-3}$, which for a given \dot{N}_{Lyc} give two different radii for the H II region(s). For lower n_0 the radiation penetrates farther, resulting in a larger R_{HII} , and conversely, for higher n_0 the radiation does not penetrate as far, and R_{HII} is smaller.

To estimate \dot{N}_{Lyc} , we use the models from D. Schaerer & A. de Koter (1997), who provide \dot{N}_{Lyc} for stars of spectral types O3–B0.5. We take the L. A. Hillenbrand (1997) census of the ONC and identify six stars that have spectral types in this range. We also sum the \dot{N}_{Lyc} of three stars (including the most massive, θ^1 Ori C) that reside in the Trapezium system, as the H II region caused by this system is likely to be larger than one driven by a single star. The different \dot{N}_{Lyc} rates from the six massive stars, and the combined \dot{N}_{Lyc} from the Trapezium system, are summarized in Table 2.

We assume that the core that will be photoeroded to form a JuMBO would ordinarily form a binary or higher-order multiple system. For simplicity, and for ease of comparison with the binary statistics of stars in the solar neighborhood, we assume that the core will fragment (or already has fragmented) into a binary star. We assume the final system mass of the binary if no photoerosion occurred would be ϵM_c (the core mass multiplied by the star formation efficiency within the core) and assume that the system splits into a primary mass m_p and a secondary mass m_s , where the mass ratio $q = m_s/m_p$ is

Table 2

Properties of the Most Massive Stars in the L. A. Hillenbrand (1997) Census of the ONC

H II Region	Star	Mass (M_{\odot})	Sp. Type	\dot{N}_{Lyc} (s^{-1})	Color
1	θ^1 Ori C	45.7	O7V	1.22×10^{49}	Red
2	θ^2 Ori A	31.2	O9V	2.88×10^{48}	Purple
3	θ^1 Ori A	18.9	O9.5V	1.78×10^{48}	Green
4	θ^1 Ori D	16.6	B0V	1.05×10^{48}	Cyan
5	HD 37061	16.3	B0V	1.05×10^{48}	Blue
6	θ^2 Ori B	12.0	B0.5V	5.09×10^{47}	Orange
7	(1 + 3 + 4)	1.40×10^{49}	Black

Note. For cross-reference with Figure 2 in Section 3, we number the H II regions; then we provide the massive star’s name, mass, and spectral type; then we calculate the Lyman continuum photon rate, \dot{N}_{Lyc} ; and finally we note the color used to represent the H II regions in Figure 2.

drawn from a flat distribution between zero and unity (M. M. Reggiani & M. R. Meyer 2011, 2013). For a core of mass M_c , the primary mass is therefore

$$m_p = \frac{\epsilon M_c}{1 + q}, \quad (5)$$

and the secondary mass is

$$m_s = qm_p, \quad (6)$$

where q is randomly selected from a flat distribution between zero and unity.

3. Results

The photoerosion mechanism described in A. P. Whitworth & H. Zinnecker (2004) is efficient within the H II region around a massive star, and to determine the potential efficacy of this mechanism in the ONC, we plot the locations and sizes of the H II regions, as well as the positions of the JuMBOs, in Figure 2.

We show two versions of this plot. In Figure 2(a), we show the positions and sizes of the H II regions when we assume the density of hydrogen nuclei in the star-forming region is $n_0 = 10^3 \text{ cm}^{-3}$. The JuMBOs (shown by the black crosses) all lie within the H II region driven by θ^1 Ori C. In contrast, when the density of hydrogen nuclei is higher ($n_0 = 10^4 \text{ cm}^{-3}$) the radii of the H II regions are much smaller (Figure 2(b)), and the majority of JuMBOs do not lie within them.

We now show the resultant mass distributions of the original cores, the photoeroded cores, and the observed masses of the

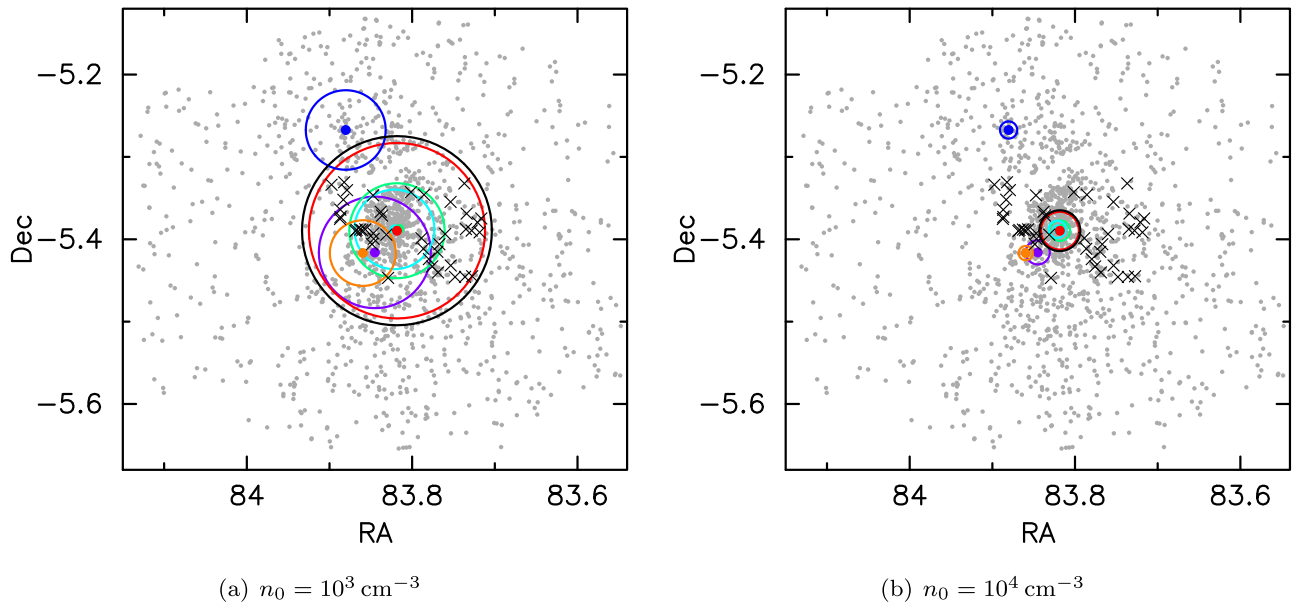


Figure 2. Radii of H II regions around six massive stars in the ONC, as well as the H II region driven by the combined flux of three massive stars within the Trapezium system (the black circles). The locations of the observed JuMBOs are shown by the black crosses. The two panels show the sizes of the H II regions for different assumed densities of hydrogen nuclei. Panel (a) shows the H II regions for the lower density ($n_0 = 10^3 \text{ cm}^{-3}$), and panel (b) shows the H II regions for the higher density ($n_0 = 10^4 \text{ cm}^{-3}$).

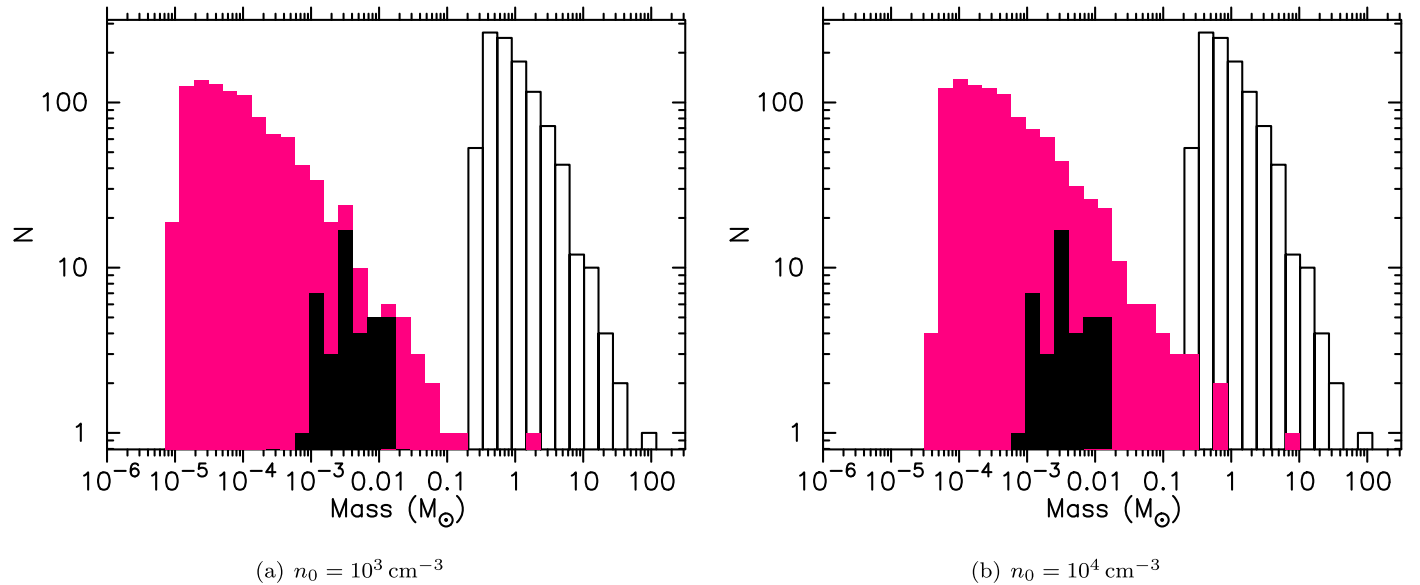


Figure 3. Histograms of the initial core mass distributions (open histograms), the masses, M_3 , of the final objects following photoerosion of the cores (pink histograms), and the observed JuMBO masses (black histograms). We show the distributions for the two different hydrogen densities. Panel (a) shows the results for lower hydrogen densities ($n_0 = 10^3 \text{ cm}^{-3}$), and panel (b) shows the results for higher hydrogen densities ($n_0 = 10^4 \text{ cm}^{-3}$).

JuMBOs in Figure 3. Again we show the results for two different assumed hydrogen densities (cf. H II region radii). The original core mass function is shown by the open histograms, and the photoeroded core masses (M_3) are shown by the solid pink histograms. For comparison, the JuMBO mass distribution is shown by the solid black histograms.

Irrespective of the assumed hydrogen density, the final M_3 masses lie comfortably within the range of the observed JuMBO masses. In the case of the lower hydrogen densities (larger H II regions, Figure 3(a)), the observed JuMBOs lie toward the high-mass end of the M_3 masses, whereas in the case of the higher hydrogen densities (smaller H II regions,

Figure 3(b)), the observed JuMBO masses lie within the center of the M_3 mass distribution.

Our underlying assumption is that the photoerosion mechanism would act upon a core that has already fragmented, or is in the process of fragmenting, into a multiple system. For simplicity we assume that the multiple system is a binary (although in reality, higher-order systems are just as, if not more, likely). In Figure 4, we plot the product of the star formation efficiency and the core mass, ϵM_c , against the final JuMBO mass, M_3 , as the purple open circles. We also plot the primary mass, m_p , if the core formed a binary star without being subject to photoerosion, against the final JuMBO mass, M_3 , as the pink asterisks.

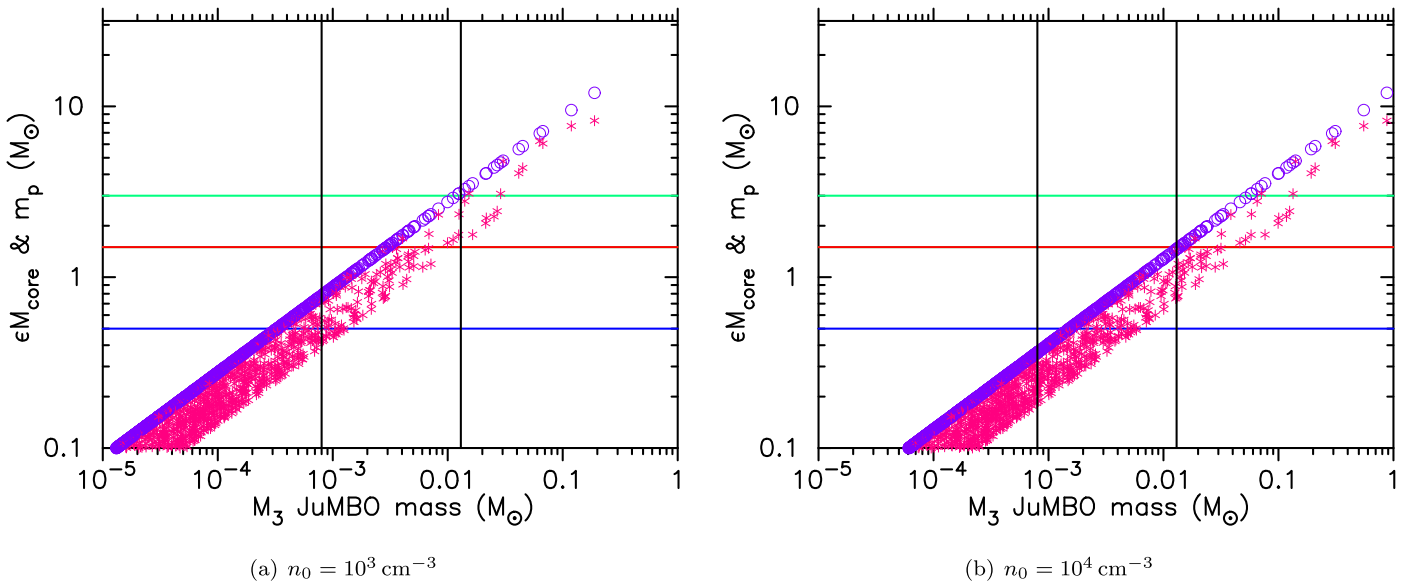


Figure 4. Product of star formation efficiency and core mass, ϵM_c , against final JuMBO mass, M_3 , shown by the purple circles. The primary mass of the binary, m_p , if it had been allowed to form without mass loss due to photoerosion, against final JuMBO mass M_3 , is shown by the pink asterisks. The lower and upper limits on the JuMBO masses from S. G. Pearson & M. J. McCaughrean (2023) are shown by the vertical black lines, and the upper limits to the primary masses, m_p , of M-type (blue), G-type (red), and A-type (green) binaries are shown by the horizontal lines. Panel (a) shows the results for lower hydrogen densities ($n_0 = 10^3 \text{ cm}^{-3}$), and panel (b) shows the results for higher hydrogen densities ($n_0 = 10^4 \text{ cm}^{-3}$).

For comparison, we show the range of observed JuMBO masses by the vertical black lines, and then the upper mass limit for primary masses of M-type (blue), G-type (red), and A-type (green) binary star systems by the horizontal lines. For the lower hydrogen densities (panel (a)), the majority of cores that form JuMBOs would have gone on to form G-type binary stars, whereas for the higher hydrogen densities (panel (b)), the initial core masses need to be lower, and so the cores that form JuMBOs would have gone on to form a mixture of M- and G-type binary systems.

4. Discussion

We have demonstrated that the photoerosion formation mechanism for substellar objects can explain the masses of the JuMBOs, and their relatively high separations (28–384 au) compared to the BD–BD binaries in the Galaxy (<10 au) if they formed from a fragmenting core that would otherwise have gone on to form a more massive (solar-type) binary or multiple system.

We draw the reader’s attention to the following caveats. First, the photoerosion theory was developed to explain single-object formation. While there is nothing to preclude its application to binary systems, we note that the compression of the prestellar core may not be as efficient if that core is already fragmenting.

Although we have shown that the initial timescales for photoerosion of the core are longer than the fragmentation timescales, and so we might expect photoerosion to act on a core that is already forming a binary or multiple system, the temperature of the core may be higher in the H II regions. There have been contradictory results in the literature on whether higher core temperatures result in reduced fragmentation (and therefore reduced/altered binary formation). S. S. R. Offner et al. (2009) note that both the Jeans length in a turbulent core and the Toomre fragmentation criterion in a disk are proportional to the gas temperature, and we would therefore

expect a higher temperature to suppress both small-scale fragmentation (see also G. Di et al. 2023) and the formation of brown dwarfs (see also M. R. Bate 2012). However, M. R. Bate (2012) finds that the binary properties (multiplicity fraction, separation distribution) are very similar in simulations with radiative transfer compared to those without.

Q.-y. Luo et al. (2022) find tentative observational evidence that in the Orion star-forming complex, the cores with the highest dust temperatures (attributed to external heating) have the lowest multiplicity fractions. Conversely, in a theoretical study, D. Guszejnov et al. (2023) find that slightly more multiple systems form in simulations with higher external radiation fields. None of these authors report a significant difference in the separation distributions in binaries that form in warmer cores.

Second, the theory assumes that photoerosion only occurs within the H II region driven by the massive star(s). This is highly dependent on the assumed density of hydrogen nuclei in the star-forming region, n_0 , with higher densities leading to smaller H II regions, and vice versa. If we assume $n_0 = 10^3 \text{ cm}^{-3}$, then $R_{\text{H II}}$ are typically $\sim 0.6 \text{ pc}$, and all of the observed JuMBOs lie within a hypothetical H II region driven by the massive stars in the Trapezium system. However, if $n_0 = 10^4 \text{ cm}^{-3}$, then $R_{\text{H II}}$ are typically $\sim 0.2 \text{ pc}$, and the vast majority of JuMBOs would not currently reside within a H II region.

Observationally, C. R. O’Dell et al. (2017) find that $\theta^1 \text{ Ori C}$ dominates the ionization of the central regions of the ONC, but $\theta^2 \text{ Ori A}$ does dominate a more distant region, suggesting the influence of $\theta^1 \text{ Ori C}$ is limited and its H II region is small. E. Habart et al. (2024) use JWST observations to establish the size of the photodissociation region around $\theta^1 \text{ Ori C}$ as $\sim 0.2 \text{ pc}$ (see also C. R. O’Dell et al. 2020) and derive a hydrogen density $n_0 \geq 10^4 \text{ cm}^{-3}$. Outside of the photodissociation region (s), observations by P. M. Weillbacher et al. (2015) suggest densities in the range $3 \times 10^3 - 2 \times 10^4 \text{ cm}^{-3}$. Both densities are still within the range over which the A. P. Whitworth & H. Zinnecker (2004) mechanism can operate.

If the H II region in the ONC is this small, this does not necessarily mean that the JuMBOs did not form within the vicinity, as they could have subsequently moved due to dynamical interactions. The ONC is one of the densest star-forming regions in the nearby (<1 kpc) Galaxy and is thought to be many dynamical timescales old (e.g., G. Furesz et al. 2008; J. J. Tobin et al. 2009; R. J. Allison & S. P. Goodwin 2011; N. Da Rio et al. 2017; J. P. Farias et al. 2020; C. Schoettler et al. 2020). R. J. Allison et al. (2010) show that the dynamical timescale of interest—the local crossing time—in the ONC is likely to be ≤ 0.1 Myr, meaning that for a typical velocity dispersion in a dynamically evolved system (~ 1 km s $^{-1}$, roughly 1 pc Myr $^{-1}$; R. J. Parker & N. J. Wright 2016), stars (and JuMBOs) can travel many parsecs in the 1–4 Myr old ONC (R. D. Jeffries et al. 2011; M. Reggiani et al. 2011; G. Beccari et al. 2017).

Furthermore, simulations that follow the photoevaporation of protoplanetary disks find a high rate of disk destruction in the ONC (F. Concha-Ramirez et al. 2019; A. J. Winter et al. 2019; R. J. Parker et al. 2021b), and this is corroborated by observations (e.g., W. J. Henney & C. R. O’Dell 1999; N. P. Ballering et al. 2023). It is entirely feasible that cores could be photoeroded within a small H II region and then migrate elsewhere in the star-forming region. In these simulations, stars whose disks are destroyed by photoevaporation move in and out of the vicinity of the massive stars(s) (R. J. Parker et al. 2021a; B. Marchington & R. J. Parker 2022).

The high probability of disk photoevaporation raises a separate issue, in that photoevaporation of the outer regions of circumstellar disks could limit the material accreted from the disk onto the central star (or binary), the quantity of which is thought to be significant (e.g., L. Hartmann et al. 1998; D. Stamatellos et al. 2011). However, even in a strong external UV radiation field such as that in the ONC, R. J. Parker et al. (2021b) show that significant mass loss from the disk occurs on timescales of 1 Myr, which are either similar to or longer than the initial core photoerosion timescales of ~ 0.3 –1 Myr derived in A. P. Whitworth & H. Zinnecker (2004). The binary is therefore likely to have assembled the majority of its mass before accretion from the disk is halted by photoevaporation of the disk, and mass loss due to photoerosion of the outer core likely dominates over any mass lost due to photoevaporation of the disk.

If the hydrogen density is low (and the corresponding H II region is large), we would expect that there should be many more lower-mass JuMBOs awaiting discovery. Conversely, if the hydrogen density is higher (and the H II region is smaller), then there should be more (as yet undiscovered) massive JuMBOs. Our analysis demonstrates that these systems would be closer in mass to M-dwarf binary systems if they were able to form without hindrance from photoerosion, and as such would have a closer separation distribution to the observed BD–BD binary systems in the field (and therefore be harder to distinguish from other substellar binaries; K. Ward-Duong et al. 2015).

5. Conclusions

We have applied the A. P. Whitworth & H. Zinnecker (2004) theory of brown dwarf formation via the photoerosion of prestellar cores by Lyman continuum radiation from massive stars to explain the JuMBOs in the ONC. The JuMBOs have component masses in the range 0.7 – $13 M_{\text{Jup}}$ and on-sky

separations of 28–384 au. We assume the Lyman continuum radiation creates a H II region around the massive stars in the ONC, and we determine both the size of the H II region and the masses of the JuMBOs that could form from photoerosion of the cores. Our conclusions are the following.

- (i) For reasonable values of the density of hydrogen nuclei (10^3 – 10^4 cm $^{-3}$), the final masses of the photoeroded cores lie comfortably within the mass range of the observed JuMBOs.
- (ii) For the lower density 10^3 cm $^{-3}$, the Lyman continuum radiation from the massive stars in the ONC would penetrate farthest and produce a H II region with a radius of ~ 0.6 pc. The observed JuMBOs all reside within this distance of the most massive stars in the ONC.
- (iii) However, the measured density of hydrogen in the ONC is $\geq 10^4$ cm $^{-3}$ (E. Habart et al. 2024), which implies a photodissociation radius no larger than 0.2 pc from the most massive stars in the ONC. The majority of the observed JuMBOs lie outside this smaller region, and at these higher densities therefore would have had to have formed within this smaller region and then migrated out due to dynamical interactions.

Irrespective of the gas density and size of the H II region, the separations of the JuMBOs are much higher than those of substellar-mass binaries (which typically peak at ~ 4 au, and presumably formed via a different mechanism). Instead, the JuMBOs are consistent with being the outcome of a photoeroded core that was already in the process of fragmenting to form a binary or multiple system.

Acknowledgments

We thank the two anonymous referees for their comments and suggestions on the original manuscript. R.J.P. acknowledges support from the Royal Society in the form of a Dorothy Hodgkin Fellowship.

ORCID iDs

Richard J. Parker  <https://orcid.org/0000-0002-1474-7848>

References

- Allison, R. J., & Goodwin, S. P. 2011, *MNRAS*, 415, 1967
- Allison, R. J., Goodwin, S. P., Parker, R. J., Portegies Zwart, S. F., & De Grijs, R. 2010, *MNRAS*, 407, 1098
- Alves, J., Lombardi, M., & Lada, C. J. 2007, *A&A*, 462, L17
- Ballering, N. P., Cleves, L. I., Haworth, T. J., et al. 2023, *ApJ*, 954, 127
- Basri, G., & Reiners, A. 2006, *AJ*, 132, 663
- Bate, M. R. 2009, *MNRAS*, 392, 590
- Bate, M. R. 2012, *MNRAS*, 419, 3115
- Beccari, G., Petr-Gotzens, M. G., Boffin, H. M. J., et al. 2017, *A&A*, 604, A22
- Bergfors, C., Brandner, W., Janson, M., et al. 2010, *A&A*, 520, A54
- Burgasser, A. J., Reid, I. N., Siegler, N., et al. 2007, in *Protostars and Planets V*, ed. B. Reipurth, D. Jewitt, & K. Keil (Tucson, AZ: Univ. Arizona Press), 427
- Chabrier, G., Johansen, A., Janson, M., & Rafikov, R. 2014, in *Protostars and Planets VI*, ed. H. Beuther et al. (Tucson, AZ: Univ. Arizona Press), 619
- Chen, X., Arce, H. G., Zhang, Q., et al. 2013, *ApJ*, 768, 110
- Clark, P. C., & Whitworth, A. P. 2021, *MNRAS*, 500, 1697
- Concha-Ramirez, F., Wilhelm, M. J. C., Portegies Zwart, S., & Haworth, T. J. 2019, *MNRAS*, 490, 5678
- Da Rio, N., Tan, J. C., Covey, K. R., et al. 2017, *ApJ*, 845, 105
- De Rosa, R. J., Patience, J., Wilson, P. A., et al. 2014, *MNRAS*, 437, 1216
- Delgado-Donate, E. J., Clarke, C. J., Bate, M. R., & Hodgkin, S. T. 2004, *MNRAS*, 351, 617
- Di, G., Sigalotti, L., Cruz, F., Hareter, M., et al. 2023, *MNRAS*, 519, 2578

- Duchêne, G., & Kraus, A. 2013, *ARA&A*, 51, 269
- Dyson, J. E. 1968, *Ap&SS*, 2, 461
- Farias, J. P., Tan, J. C., & Eyer, L. 2020, *ApJ*, 900, 14
- Fuzesz, G., Hartmann, L. W., Megeath, S. T., Szentgyorgyi, A. H., & Hamden, E. T. 2008, *ApJ*, 676, 1109
- Gahm, G. F., Grenman, T., Fredriksson, S., & Kristen, H. 2007, *AJ*, 133, 1795
- Goodwin, S. P., Kroupa, P., Goodman, A., & Burkert, A. 2007, in *Protostars and Planets V*, ed. B. Reipurth, D. Jewitt, & K. Keil (Tucson, AZ: Univ. Arizona Press), 133
- Goodwin, S. P., & Whitworth, A. P. 2007, *A&A*, 466, 943
- Goodwin, S. P., Whitworth, A. P., & Ward-Thompson, D. 2004, *A&A*, 414, 633
- Guszejnov, D., Raju, A. N., Offner, S. S. R., et al. 2023, *MNRAS*, 518, 4693
- Habart, E., Peeters, E., Berné, O., et al. 2024, *A&A*, 685, A73
- Hartmann, L., Calvet, N., Gullbring, E., & D'Alessio, P. 1998, *ApJ*, 495, 385
- Haworth, T. J., Facchini, S., & Clarke, C. J. 2015, *MNRAS*, 446, 1098
- Hennebelle, P., & Chabrier, G. 2013, *ApJ*, 770, 150
- Henney, W. J., & O'Dell, C. R. 1999, *AJ*, 118, 2350
- Hester, J. J., Scowen, P. A., Sankrit, R., et al. 1996, *AJ*, 111, 2349
- Hillenbrand, L. A. 1997, *AJ*, 113, 1733
- Janson, M., Hormuth, F., Bergfors, C., et al. 2012, *ApJ*, 754, 44
- Jeffries, R. D., Littlefair, S. P., Naylor, T., & Mayne, N. J. 2011, *MNRAS*, 418, 1948
- Kahn, F. D. 1969, *Phy*, 41, 172
- Kang, S.-J., Kerton, C. R., Choi, M., & Kang, M. 2017, *ApJ*, 845, 21
- Lazzoni, C., Rice, K., Zurlo, A., Hinkley, S., & Desidera, S. 2024, *MNRAS*, 527, 3837
- Luo, Q.-y., Liu, T., Tatematsu, K., et al. 2022, *ApJ*, 931, 158
- Marchington, B., & Parker, R. J. 2022, *MNRAS*, 515, 5449
- Maschberger, T. 2013, *MNRAS*, 429, 1725
- Mathew, S. S., & Federrath, C. 2021, *MNRAS*, 507, 2448
- O'Dell, C. R., Abel, N. P., & Ferland, G. J. 2020, *ApJ*, 891, 46
- O'Dell, C. R., Kollatschny, W., & Ferland, G. J. 2017, *ApJ*, 837, 151
- Offner, S. S. R., Hansen, C. E., & Krumholz, M. R. 2009, *ApJ*, 704, L124
- Offner, S. S. R., Kratter, K. M., Matzner, C. D., Krumholz, M. R., & Klein, R. I. 2010, *ApJ*, 725, 1485
- Padoan, P., & Nordlund, A. 2004, *ApJ*, 617, 559
- Parker, R. J., Alcock, H. L., Nicholson, R. B., Panić, O., & Goodwin, S. P. 2021a, *ApJ*, 913, 95
- Parker, R. J., & Goodwin, S. P. 2011, *MNRAS*, 411, 891
- Parker, R. J., Nicholson, R. B., & Alcock, H. L. 2021b, *MNRAS*, 502, 2665
- Parker, R. J., & Wright, N. J. 2016, *MNRAS*, 457, 3430
- Pearson, S. G., & McCaughrean, M. J. 2023, arXiv:2310.01231
- Pollack, J. B., Hubickyj, O., Bodenheimer, P., et al. 1996, *Icar*, 124, 62
- Portegies Zwart, S., & Hochart, E. 2024, *ScPA*, 3, 001
- Raghavan, D., McMaster, H. A., Henry, T. J., et al. 2010, *ApJSS*, 190, 1
- Rees, M. J. 1976, *MNRAS*, 176, 483
- Reggiani, M., Robberto, M., Da Rio, N., et al. 2011, *A&A*, 534, A83
- Reggiani, M. M., & Meyer, M. R. 2011, *ApJ*, 738, 60
- Reggiani, M. M., & Meyer, M. R. 2013, *A&A*, 553, A124
- Reipurth, B., & Clarke, C. 2001, *AJ*, 122, 432
- Rice, W. K. M., Lodato, G., & Armitage, P. J. 2005, *MNRAS*, 364, L56
- Salpeter, E. E. 1955, *ApJ*, 121, 161
- Schaerer, D., & de Koter, A. 1997, *A&A*, 322, 598
- Schoettler, C., de Bruijne, J., Vaher, E., & Parker, R. J. 2020, *MNRAS*, 495, 3104
- Stamatellos, D., & Whitworth, A. P. 2009, *MNRAS*, 392, 413
- Stamatellos, D., Whitworth, A. P., & Hubber, D. A. 2011, *ApJ*, 730, 32
- Thies, I., & Kroupa, P. 2007, *ApJ*, 671, 767
- Tobin, J. J., Hartmann, L., Fuzesz, G., Mateo, M., & Megeath, S. T. 2009, *ApJ*, 697, 1103
- Wang, Y., Perna, R., & Zhu, Z. 2024, *NatAs*, 8, 756
- Ward-Duong, K., Patience, J., & De Rosa, R. J. 2015, *MNRAS*, 449, 2618
- Weilbacher, P. M., Monreal-Ibero, A., Kollatschny, W., et al. 2015, *A&A*, 582, A114
- Whitworth, A. P., & Zinnecker, H. 2004, *A&A*, 427, 299
- Winter, A. J., Clarke, C. J., Rosotti, G. P., Hacar, A., & Alexander, R. 2019, *MNRAS*, 490, 5478